

Precise Visual-Inertial Localization for UAV with the Aid of A 2D Georeferenced Map

MAO Jun, ZHANG Lilian, HE Xiaofeng, QU Hao, HU Xiaoping

Abstract— Precise geolocalization is crucial for unmanned aerial vehicles (UAVs). However, most current deployed UAVs rely on the global navigation satellite systems (GNSS) or high precision inertial navigation systems (INS) for geolocalization. In this paper, we propose to use a lightweight visual-inertial system with a 2D georeference map to obtain accurate and consecutive geodetic positions for UAVs. The proposed system firstly integrates a micro inertial measurement unit (MIMU) and a monocular camera as odometry to consecutively estimate the navigation states and reconstruct the 3D position of the observed visual features in the local world frame. To obtain the geolocation, the visual features tracked by the odometry are further registered to the 2D georeferenced map. While most conventional methods perform image-level aerial image registration, we propose to align the reconstructed points to the map points in the geodetic frame; this helps to filter out the large portion of outliers and decouples the negative effects from the horizontal angles. The registered points are then used to relocalize the vehicle in the geodetic frame. Finally, a pose graph is deployed to fuse the geolocation from the aerial image registration and the local navigation result from the visual-inertial odometry (VIO) to achieve consecutive and drift-free geolocalization performance. We have validated the proposed method by installing the sensors to a UAV body rigidly and have conducted two flights in different environments with unknown initials. The results show that the proposed method can achieve less than 4m position error in flight at 100m high and less than 9m position error in flight about 300m high.

I. INTRODUCTION

The navigation system is the key component that supports the UAVs to perform various tasks such as search and rescue, surveying and mapping. Currently, most UAVs integrates an INS with the GNSS to obtain consecutive and precise motion state estimation. However, the GNSS signals are subjected to interference and multipath propagation, which can cause the navigation precision to fall dramatically; this is more notable for small UAVs which only equipped with MIMUs.

With the development of computer vision, visual navigation techniques have been widely deployed in UAVs. Well-developed visual navigation algorithms have achieved notable precision. The field of visual navigation comprises two main approaches: relative visual localization (RVL) and absolute visual localization (AVL) [1]. The RVL algorithms include visual odometry (VO) and visual simultaneous localization and mapping (VSLAM). VO estimates the relative motion between two consecutive frames or keyframes, and

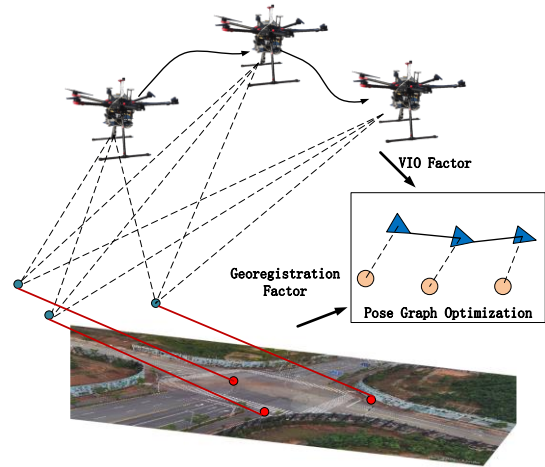


Figure 1. The proposed method uses VIO reconstructed 3D points to perform georegistration, and uses a pose graph to fuse the VIO and geolocalization results to achieve consecutive, drift-free precise localization performance.

then integrates the relative motion to obtain the position and altitude of the agent [2]. However, the errors in each relative motion estimation accumulate with the integration process. To reduce the drifts, IMUs have been combined with cameras to form visual-inertial odometry (VIO) [3]. VO or VIO also act as a component in a VSLAM system, which jointly estimates the vehicle's position and reconstructs the 3D position of the observed landmarks [4][5]. While the vehicle returns to an explored area, VSLAM can perform loop closure to reduce the accumulated drift from odometry and adjust the constructed map.

The development of RVL techniques has powered wide applications of UAVs. However, visual odometry suffers from accumulated drifts; though loop closure in VSLAM can reduce the drifts, it requires the vehicle to travel back to previously explored areas, which is not efficient and safe in some situations. Furthermore, in many applications, the UAVs are desired to navigate to desired locations represented by latitudes and longitudes; however, without known initial position and orientation, RVL is not capable to locate the vehicle in the geodetic frames.

In contrast to RVL techniques, AVL compares the camera images with a map to localize the vehicle. When the map is aligned with the geodetic frame, the output of AVL is the geodetic location; moreover, there is no integration operation

*All authors are with the College of Intelligence Science and Technology, National University of Defense Technology, Changsha, China. Corresponding author to maojun12@nudt.edu.cn. Research supported by the National Nature Science Foundation of China under Grant 62073331 and 61773394

in AVL, which brings in the advantage of drift-free position estimation. The availability of georeferenced maps from online platforms, such as Google Earth and Bing map, has also motivated the research of AVL [6][7][8].

In UAV applications, template matching and feature matching are two commonly used approaches to register the aerial images with the georeferenced map image to achieve AVL performance [1]. However, most existing work only performs image-level registration, where the camera images are treated as a patch from the map image. To obtain similar downward-looking camera images, gimbals have been used to decouple the negative effects of the horizontal angles [6][7][9][10] and known initial positions [6][7][8][9][11][12] are required to achieve good performances. However, current UAVs usually equipped with multiple sensors distributed on different parts of the UAV body (such as the front view camera for obstacle avoidance and the downward-looking camera for localization), using a gimbal installation makes it hard to integrate sensors at different parts. Moreover, known initial positions are not easy to obtain; in many challenging situations, the vehicle has to localize itself with unknown initials or kilometer scale initial uncertainties.

In this paper, we provide a novel approach that combines a RVL and an AVL technique to obtain an accurate and consecutive estimation of the UAV's geolocations. The proposed algorithm consists of three components: a visual-inertial odometry, a feature-based image registration component and a pose graph fusion component. Unlike most conventional geolocalization methods that focus on image-level registration [6][7][8][9][12] or utilize a 3D georeferenced model [11], the proposed method uses a 2D map and makes use of the VIO reconstructed 3D points to perform georegistration. Moreover, we propose to use a pose graph to fuse the VIO and the georegistration results to obtain consecutive and drift-free localization in the geodetic frame. The proposed approach is exemplified in Fig.1.

The main contributions of this work are as follows:

1. We propose a novel aerial image registration method that utilizes the VIO reconstructed 3D points to perform georegistration on the geodetic frame.
2. We introduce a framework for UAV that integrates the VIO and the aerial image registration results to achieve consecutive, drift-free and precise geolocalization performance.
3. We conduct real flight experiments with different motion states and in different visual environments. We also make comparisons with conventional methods to highlight the effectiveness of the proposed method.

The paper proceeds as follows: Section II reviews the related research. Section III presents the detailed approach. Sections IV and V demonstrate the experimental procedure and experimental results respectively, with the conclusions drawn in Section VI

II. BACK GROUNDS

The navigation system is the basic component that powers the UAV to complete complex tasks. In recent years, vision-based navigation techniques have received increasing focus, as they only use lightweight sensors and do not need to receive

electromagnetic signals. Existing visual navigation techniques can be broadly categorized as RVL and AVL [1].

VO [2] and VSLAM [13] are two widely used RVL approaches, where VO usually acts as a component in VSLAM. Noticeable vision-only relative localization algorithms include SVO [14], DSO [15] and ORB-SLAM [16]. To improve the accuracy and robustness of the vision system, other sensors have been proposed to integrate with the cameras. One of the most notable methods is to integrate IMUs with cameras, as IMU can provide high rate, robust motion estimation and vision can provide relative precise motion estimation. VINS [4] and ORB-SLAM3 [5] are representatives of the current visual-inertial techniques. VO and VSLAM can estimate the position of the vehicle and simultaneously reconstruct the position of the tracked features. However, RVL is not capable to estimate the absolute position relative to the geodetic frame unless the initial geodetic position and orientation are given. Moreover, VO suffers from accumulated errors and VSLAM requires loop closures to achieve accurate localization and mapping; this limits the application of UAV in situations where precise and efficient absolute navigation is required.

The AVL techniques aim to register the onboard camera images to a reference map to estimate the position. When the database is aligned with the geodetic frame, the geodetic position can then be obtained. For UAV applications, georeferenced maps captured by satellites [9][7][6][8][12] or other vehicles [17] have been widely used. Template matching is a long-developed technique to perform aerial imagery registration. Template matching methods treat the query camera image as a patch extract from the georeferenced map, therefore it firstly warps the image to a similar scale and orientation with the map, and then compares with different parts of the map. Normalized cross-correlation (NCC) [9][8], mutual information (MI) [18], normalized information distance (NID) [7] and other similarity parameters are used in template matching aerial image registration. Due to the computation costs of template similarity, an initial guess of the position is usually required to reduce the search space. As template matching methods are sensitive to orientation variations and horizontal angles, gimbals have been used to capture downward-looking camera images with fixed orientation [9][18][7].

An alternative AVL approach is to match the sparse features between the camera image and the reference map. Conte [19] used edge features for aerial image registration, but the results have shown low match rates. [10] proposed a novel feature named as abBRIEF, which was a modified version of BRIEF feature [20], for AVL implementation and has shown better performance than the conventional BRIEF feature. [17] used a self-constructed 3D landmark map as the reference, where the visual landmarks were described as BRISK features [20]; in the localization stage, they used weak GPS priors to reduce visual aliasing. [21] built a HOG feature lookup table, which contains HOG features extracted at every map pixel; their method requires no prior location information as the initial stage contains a global search process. Nassar [12] proposed to use SIFT features for aerial image registration, which is then followed with a semantic feature alignment to localize the vehicle. Bianchi [6] trained an autoencoder to describe the camera and map image; with the aid of prior location information, their method has shown high localization

rate and low localization error in different periods of a day. To reduce visual confusion, gimbals and known initials have also been used in feature-based aerial image registration methods [6][12][19].

In summary, VO suffers from drifts and VSLAM subjects to loop closures, while AVL is hard to register every query camera image to the referenced map due to the visual appearance variations the imperfect design of the match algorithms. In this paper, we propose to integrate visual-inertial odometry with a feature-based AVL component. The odometry can generate consecutive and smooth relative navigation results, while the AVL can transfer the relative navigation result to the geodetic frame and cure the VIO drifts. Our method is closely related to [11], which not only integrated RVL and AVL in a factor graph, but also used 3D landmarks for georegistration. However, the authors in [11] used a tactical level IMU for dead reckoning and used a 3D model as the reference, which is expensive and hard to obtain. In this paper, we integrate a MIMU and a camera to achieve a low cost and light-weighted navigation system. Furthermore, we only use a 2D map as the reference which is easier to obtain than the 3D model. Unlike most conventional methods that have used a gimbal and known initials, we work with unknown initials and rigidly mounted sensors; this can power the UAV applications in challenging environments and helps to integrate with the sensors distributed at different body parts of the vehicle.

III. METHODOLOGY

The proposed method consists of three main components: the sliding-window VIO for relative navigation, the aerial image registration component for geolocalization and the pose graph for information fusion. The VIO integrates a MIMU and a monocular camera to estimate the motion states and reconstruct the 3D position of the tracked visual features in the local world frame. The aerial image registration part firstly extracts map features in an offline process; in the online localization process, it uses a magnetic compass to aid the computation of the camera image feature descriptors and utilizes the reconstructed 3D points from the VIO to filter out the outlier matches. The matched points are then transferred to the geodetic frame and then the PNP (Perspective-N-Point) algorithm is used to relocate the vehicle. The pose graph optimization component fuses the relative navigation results from the VIO with the geodetic positions from the aerial image registration component to achieve consecutive and drift-free geolocalization performance.

A. Relative Visual Localization with a Sliding Window VIO

We adapt the VINS-Mono [4], which is a state of the art visual-inertial odometry, as the RVL component in the proposed system. The VIO can estimate the navigation parameters (e.g. position, attitude and velocity) and simultaneously reconstructs the 3D position of the tracked points in the local world frame W . The full state vector of the VIO is defined as:

$$\begin{aligned} \mathcal{X} &= [\mathbf{x}_0, \mathbf{x}_1, \dots, \mathbf{x}_n, \lambda_0, \lambda_1, \dots, \lambda_i] \\ \mathbf{x}_k &= [\mathbf{p}_{B_k}^W, \mathbf{v}_{B_k}^W, \mathbf{q}_{B_k}^W, \mathbf{b}_a, \mathbf{b}_g], k \in [0, n] \end{aligned} \quad (1)$$

where \mathbf{x}_k is the IMU body state at the k -th keyframe in the sliding window; it contains the position vector $\mathbf{p}_{B_k}^W$, the

velocity vector $\mathbf{v}_{B_k}^W$, the quaternion $\mathbf{q}_{B_k}^W$, the accelerometer bias \mathbf{b}_a and the gyroscope and bias \mathbf{b}_g . λ_i is the inverse depth of the i -th feature tracked in the sliding window. Based on λ_i , the 3D position of the feature in the local world frame can be obtained as:

$$\mathbf{P}_i^W = \mathbf{R}_{B_k}^W (\mathbf{R}_C^B \frac{1}{\lambda_i} \pi_c^{-1} \begin{bmatrix} u_i^{C_k} \\ v_i^{C_k} \end{bmatrix}) + \mathbf{p}_C^B + \mathbf{p}_{B_k}^W \quad (2)$$

where $[u_i^{C_k}; v_i^{C_k}]$ is the first observation of the i -th feature in the window; π_c^{-1} is the back projection function that turns the pixel location into a unit vector using the camera intrinsic parameters. \mathbf{R}_C^B and \mathbf{p}_C^B are the extrinsic parameters between the IMU and the camera. In our implementation, we calibrated the extrinsic parameters offline and frozen them during the navigation process.

Note that, without the knowledge of the starting position, the VIO can only estimate the motion states related to the local world frame. Moreover, the integration process causes the VIO accuracy to degrade with the travel distance. In a VSLAM system, a loop closure component is used to detect previously explored areas, which is then used to relocate the vehicle and adjust the constructed map. However, loop closure only reduces the relative navigation errors and requires travelling back to previously visited places.

B. Geolocalization by Aerial Image Registration

Prebuilt georeferenced maps contain rich features that can be used as landmarks for absolute visual navigation. The main challenge of using the georeferenced maps lies in the feature registration process. In this paper, we develop a novel feature-based registration method for localization, which makes use of the VIO tracked features and describes them with SIFT descriptor [22] for implementation. Other features can also be used in aerial image registration; however, the scope of this paper is to investigate the advantage of using the reconstructed 3D points in geolocalization and the SIFT feature is adopted as an example.

1) Map Preprocessing

Offline map processing is the first step of the proposed aerial image registration component. As the onboard camera images and the reference maps can have very different quality, the repetitiveness of the feature detector cannot be guaranteed. Therefore, we extract interest points with a constant stride (10 pixels in our experiments) in the map to ensure that the observed camera features are included in the map feature database; SIFT keypoints are then constructed at the interest points with fixed orientation and size. Later in the online registration process, camera images are rotated and resized to have similar orientation and scale as the map with the aids of the orientation from the magnetic compass and the measured height from the VIO; then SIFT points are also built at the VIO tracked corner points with the same feature orientation and size as the map features to preserve the consistency. The offline map processing component generates a reference feature database represented as:

$$\mathbf{D} = \{(\mathbf{f}_j^m, \mathbf{l}_j^m)\}_j \quad (3)$$

where f_j^m is the feature descriptor to the j-th map feature, and l_j^m is the 2D geodetic position of the j-th feature.

When anchoring the origin of the geodetic frame at the point corresponding to the map's left-up corner and define the geodetic frame as ENU (East-North-Up) orientation, l_j^m can be expressed as:

$$l_j^m = [u_j^m \cdot \sigma^m; -v_j^m \cdot \sigma^m] \quad (4)$$

where $[u_j^m; v_j^m]$ is the detected feature position on the map and σ^m is the ratio of the map.

2) Image Feature Extraction

Comparing to some existing works that use a separated feature registration process to the dead reckoning component [9][11][19], we propose to use the VIO tracked features for registration. This not only reduces the time consumption for image feature detection, but also helps to incorporate the 3D reconstruction information to augment the registration performance.

Instead of using all the feature points, we only select the points that have a reprojection error smaller than a predefined threshold for registration. If the number of the selected points are below a threshold, we skip the image frame. Once enough good reconstructed 3D points are available, the corresponding camera image is rotated with the aid of the magnetic compass, and rescaled to the map's scale base on the measured height from the VIO. The position of the tracked points on the new image can be calculated as:

$$\begin{aligned} \begin{bmatrix} u_i^c \\ v_i^c \end{bmatrix} &= s \mathbf{R}_{2D}(\theta_{mag}) \begin{bmatrix} u_i^c \\ v_i^c \end{bmatrix} \\ s &= \frac{\sigma^m}{\sigma^c} \approx \sigma^m \frac{f}{H} \end{aligned} \quad (5)$$

where $[u_i^c; v_i^c]$ is the feature observation at the camera image and $[u_i^c; v_i^c]$ is the corresponding observation at the rotated and scaled image. $\mathbf{R}_{2D}(\theta)$ is the 2D rotation operation, which related to the compass orientation θ_{mag} . s is the image scale factor, which is related to the ratio of the map σ^m , the camera focal length f and the VIO measured altitude H .

SIFT descriptors are then extracted from the rotated and scaled image with fixed orientation and scale as the map features. The construct the query features in the k-th camera image are represented as:

$$Q_k = \{(f_i^c, P_i^W)\}_l \quad (6)$$

where f_i^c is SIFT descriptor and P_i^W is reconstructed 3D points shown in (2).

3) Feature Matching and Geolocalization

The proposed feature matching process includes two steps: finding raw feature correspondence and filtering outliers. The raw matches are built by finding the best image feature correspondence in the map database. After feature matching, previous work [9][12][21][23] has considered that the camera image can be overlaid to the reference map with a 2D translation and rotation operation; this assumption is valid for cameras installed on a gimbal; however, for cameras with a rigid installation, the horizontal angles can lead to accuracy degradation. In this work, we focus on working with rigidly mounted sensors, as such installation helps to integrate with sensors distributed at other parts of the UAV.

Instead of aligning the camera image to the reference map, we propose to align the reconstructed 3D points to the map points in the geodetic horizontal level. Thanks to the use of IMU, the VIO is capable to align the local world frame with the horizontal plane at the initialization process. Therefore, the reconstructed 3D points are decoupled from the negative effects of the horizontal angles. The reconstructed points are firstly rotated to have the same direction as the geodetic frame as:

$$P_i^{\tilde{G}} = \mathbf{R}_{3D}(\theta_{mag}, \theta_{vio}) P_i^W \quad (7)$$

where θ_{mag} is the orientation measured by the compass, and θ_{vio} is the relative heading to the local world frame, which is measured by the VIO. $\mathbf{R}_{3D}(\cdot)$ represents the corresponding 3D rotation.

After the rotation as shown in (7), the 3D points can be aligned to the map points in the geodetic horizontal plane. To find the best translation vector that aligns the points, we compute the 2D translation vector for every correspondence as:

$$t_{i,j} = l_j^m - P_i^{\tilde{G}}(x, y) \quad (8)$$

where the j-th map feature and the i-th image feature is a correspondence, and $P_i^{\tilde{G}}(x, y)$ means the 2D vector consists of the first two elements.

Then for every match, we count the number of the inlier correspondences, where a match is considered as an inlier if its translation vector has a variation smaller than a set threshold. For the match that have the most inliers and the inlier number is higher than an acceptance threshold, we consider it is a successful registration and average all the inliers' translation vector for use. The translation vector is regarded as the position drift in the geodetic frame. Therefore, for all the inliers, the obtained position translation vector is used to move the points to align with the geodetic frame as:

$$P_i^G = P_i^{\tilde{G}} + t \quad (9)$$

where the first two elements of t are the averaged 2D translation from all inliers, and the third element is zero.

At this point, the inliers are moved to align with the geodetic frame in the horizontal level. The absolute position and altitude of the camera can be calculated by using the PNP algorithm, and the absolute position of the IMU body frame can be expressed as:

$$p_{B_k}^G = p_{C_k}^G - \mathbf{R}_{C_k}^G p_C^B \quad (10)$$

where $p_{C_k}^G$ and $\mathbf{R}_{C_k}^G$ are obtained from the PNP algorithm.

C. Global Pose Graph Optimization

The mentioned VIO in section III.A only estimates the relative navigation parameters and is suffered from drifts, while the aerial image registration in section III.B only provides geodetic position at the matched places. To achieve consecutive and drift-free geolocalization performance, we propose to integrate the VIO and the aerial image registration results to complement each other.

In the pose graph, each node represents the state vector containing the position and attitude of the vehicle, which is represented as:

$$n_k = [p_{B_k}^G, q_{B_k}^G], \quad k \in [0, n] \quad (11)$$

The VIO outputs are used to construct the relative edges that describe the relative transformation between two nodes as:

$$\hat{\mathbf{r}}_{ij}^{B_i} = (\hat{\mathbf{R}}_{B_i}^W)^{-1} (\hat{\mathbf{p}}_{B_j}^W - \hat{\mathbf{p}}_{B_i}^W); \quad \hat{\mathbf{q}}_{ij} = \hat{\mathbf{q}}_{B_j}^R \otimes (\hat{\mathbf{q}}_{B_i}^R)^{-1} \quad (12)$$

where the hat represents the estimation from the VIO and \mathbf{R} represents the rotation matrix corresponding to the quaternion. The residual factor can then be given as:

$$r_{ij}(\mathbf{q}_{B_i}^G, \mathbf{p}_{B_i}^G, \mathbf{q}_{B_j}^G, \mathbf{p}_{B_j}^G) = \begin{bmatrix} (\mathbf{R}_{ij}^G)^{-1} (\mathbf{p}_{B_j}^G - \mathbf{p}_{B_i}^G) - \hat{\mathbf{p}}_{ij}^{B_i} \\ \boldsymbol{\theta}_{ij} - \hat{\boldsymbol{\theta}}_{ij} \end{bmatrix} \quad (13)$$

where $\boldsymbol{\theta}_{ij}$ is the imaginary part of the quaternion \mathbf{q}_{ij} .

The geodetic positions from the aerial image registration are used to construct the absolute edges and the residual factor is expressed as:

$$r_i(\mathbf{p}_{B_i}^G) = \mathbf{p}_{B_i}^G - \hat{\mathbf{p}}_{B_i}^G \quad (14)$$

where $\hat{\mathbf{p}}_{B_i}^G$ represents the position from georegistration as shown in (10). Note that, the absolute edges are only available for the successfully registered frames.

The whole graph is optimized by minimizing the following cost function:

$$\min_{\mathbf{p}_{i,j}^G, \mathbf{q}_{i,j}^G} \left\{ \sum_{(i,j) \in \mathcal{S}} \|\mathbf{r}_{ij}\|_{\mathcal{S}}^2 + \sum_{(i,j) \in \mathcal{L}} \rho(\|\mathbf{r}_i\|_{\mathcal{L}}^2) \right\} \quad (15)$$

where \mathcal{S} is the set of all the relative edge factors and \mathcal{L} is the set of all the absolute edges; $\boldsymbol{\Sigma}$ and $\boldsymbol{\Omega}$ is the information matrix of the edges, and $\rho(\cdot)$ is the Huber norm. The use of the Huber norm in (15) helps to reduce the impact of possible wrong aerial image registrations.

IV. EXPERIMENTAL SETUP

A. System setup

The experiments were conducted by rigidly mounting the navigation system to a DJI M600Pro UAV as shown in Fig.2. The system consists of a downward-looking monocular camera, a MIMU, a magnetic compass and a GNSS receiver. The vehicle was also equipped with a polarized light compass for further research. Note that the polarized light compass was equipped at the top of the vehicle as shown in Fig.2.



Figure 2. The used UAV and navigation system in the experiments

B. Datasets

Two datasets were used to testify the algorithms: The Rural dataset and the Testing Zone dataset. For each dataset, we conducted one flight for validation. The used 2D georeferenced maps were constructed by camera images

captured by another UAV with a time separation longer than 3 months. The used maps have a resolution of 0.3 meter/pixel as shown in Fig.5. The geodetic frame was anchored at the left-up corner of the map, with the orientation defined as ENU as described in Section III

In the online navigation process, the camera worked at a frame rate of 10Hz, the MIMU worked at 200 Hz. The GNSS receiver worked at 10 Hz and was integrated with the MIMU to obtain the ground truth.

The Rural dataset covers an area of 0.51 km \times 0.4 km located in Changsha, China. Most of the area along the flight trajectory is covered by nature features, such as trees and grassland, with a few buildings and roads, as shown in Fig.5(a). The average height of this flight was about 110 meters above the ground. The flight lasted for about 6 minutes with a length of 1.18 kilometers.

The Test Zone dataset contains an area of 1.46 km \times 1.45 km at the National Intelligent Connected Vehicle (Changsha) Testing Zone. The Zone contains city subzones, high way subzones and urban subzones, as shown in Fig.5(b). The average height of this flight was about 285 meters, and the flight lasted for about 7 minutes with a length of 2.45 kilometers.

The details of the two datasets are shown in Table.I. Note that, the two flights captured images of various natural visual appearances with different fly speed and height, which make them valid to test the algorithm in different conditions.

TABLE. I DETAIL OF THE CONDUCTED FLIGHTS

Dataset	Time (s)	Length(km)	Avg Height(m)	Avg Horizontal Angle (°)
Rural	448.20	1.18	110	5.63
Testing Zone	407.50	2.45	285	7.80

C. Experimental Procedure

For algorithm validation, we extracted the map points with a constant 10-pixels' stride and detect the camera image points as described in [4]. In all, there were 22,042 map features in the Rural dataset and 116,354 map features in the Testing Zone dataset. To speed up the feature matching process, we used the FLANN-based matcher [24] to find the best match for every query feature.

TABLE. II DETAIL OF THE CONDUCTED AERIAL IMAGE REGISTRATION METHOD

Method	Feature Detector	Feature Descriptor	Registration Method
Proposed	Camera: Shi-Tomasi corner feature Map: extract with every 10 pixels' stride	SIFT descriptor with fixed orientation and size	Align the reconstructed 3D points to the map points in the geodetic horizontal level
M1	Camera: Shi-Tomasi corner feature Map: extract with every 10 pixels' stride	SIFT descriptor with fixed orientation and size	Align the camera image with the map image
M2	SIFT detector for both the camera images and the map images	SIFT descriptor with parameters set by the detector	Align the camera image with the map image

Two image registration methods were used for comparison. The first method (M1) performs image-level registration, where an image translation was searched to best align the rotated and scaled camera image with the map; this obtained image translation was then mapped to position translation to compensate for the localization drifts. Such an aerial image registration strategy for geolocalization has been used in both the template matching methods [8][18] and the feature matching methods [12][23]. The second method (M2) also uses the same registration process, but SIFT feature detector was used at the front end to find interest points and automatically set the SIFT feature parameters for both the camera images and the map image; this method is consistent with conventional image registration method where feature detectors have been used to automatically find interest points in both the query and the reference images [12][23]. The details of the proposed method and the two conventional methods are shown in Table II.

V. EXPERIMENTAL RESULTS

As the VIO component has been studied comprehensively in [4], here we present the performance of the aerial image registration component and the pose graph component to demonstrate the effectiveness of the proposed method.

A. Aerial Image Registration Performance

The aerial image registration performance of the three conducted methods is presented in this section. Fig.3 shows the true match rate of the three methods, where a true match requires at least eight inlier matches and the registered place is within 30 meters to the ground truth location.

In both the Rural dataset and the Testing Zone dataset, M1 shows a higher match rate than M2. The premise of a successful image registration requires the detector to find out the same features in both the query and the reference images with similar feature parameters. However, the camera and map images were captured at different times with different cameras; this is challenging for the SIFT feature detector to detect consistency features in the two source images. Therefore, M2 shows a lower true match rate than M1 in both the Rural and the Testing Zone datasets due to the usage of the automatic feature detector, as described in Table.II.

Though the proposed method and M1 use the same features for image registration, they show different performance as shown in Fig.3. In the Rural dataset, the vehicle flew at a low speed and altitude with small horizontal angles as shown in Table.II; in this situation, the relation between the scaled and rotated camera images and the map image can be regarded as a pure image translation, and M1 can achieve a high match rate. Moreover, as M1 uses all the camera image features, it achieves a slightly better performance than the proposed method, which only selects the points with a small reprojection error for use. In the Testing Zone dataset, the flight height, speed, and horizontal angles are larger than those in the Rural dataset; this is more challenging for M1 as pure translation is not adequate to describe the relations between the camera images and the map image. Benefit from using the VIO reconstructed 3D points, which is horizontally aligned with the geodetic frame, the proposed method achieves a much higher match rate than M1.

Fig.4 shows the position root mean square error (RMSE) of the true matches of the three conducted methods. As both

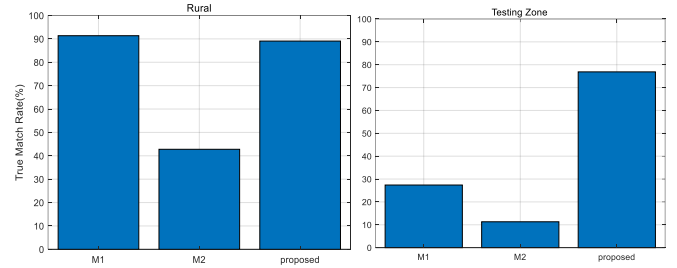


Figure 3. The match rate of the three conducted methods in the Rural and the Testing Zone datasets. The proposed method shows a consistent high match rate in both datasets.

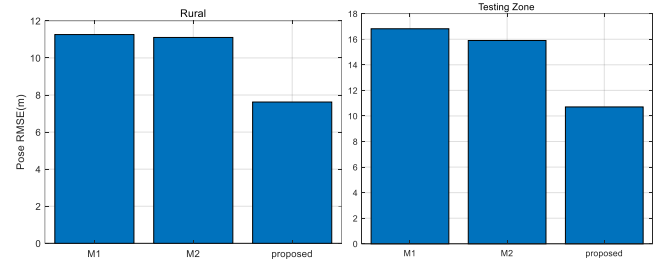


Figure 4. The geolocalization error in the Rural and the Testing Zone datasets. The proposed method achieves the best performance in both datasets.

M1 and M2 perform image-level registration, their accuracy is comparable in the two datasets. We highlight that the proposed aerial image registration method shows the best localization precision in both the Rural and the Testing Zone datasets, which demonstrates the performance improvements brings in by using the reconstructed 3D points. Note that, the proposed method's localization error in the Testing Zone dataset is larger than that in the Rural dataset; this is mainly due to the flight height in the Testing Zone dataset is higher, which is more challenging for 3D reconstruction.

In summary, Fig.3 and Fig.4 show that the proposed registration method has a consistent high match rate and the smallest localization error in the testing datasets. We also investigated the time consumption of the image registration component in a computer with a 2.60GHz Intel i7-6700HQ processor and 16GH RAM. The code was ran as a ROS node. In the Rural dataset, the average georegistration time was about 15.6 milliseconds per frame; in the Testing Zone dataset, it took about 216.3 milliseconds to process one frame. Further improvements, such as using the previous localization result to bound the feature search area, can reduce the time consumption.

B. Localization Performance by Fusing the VIO with the Georegistration

The final localization output of the proposed system is obtained by fusing the relative localization result from the VIO and the geodetic position from the aerial image registration. To highlight the advantage of fusing the relative and absolute localization techniques, we present the precision of the

TABLE.III LOCALIZATION PERFORMANCE

Dataset	VIO Pose RMSE(m)	Registration Pose RMSE(m)	Fusion Pose RMSE(m)
Rural	28.43	7.406	3.76
Testing Zone	73.62	10.70	8.75

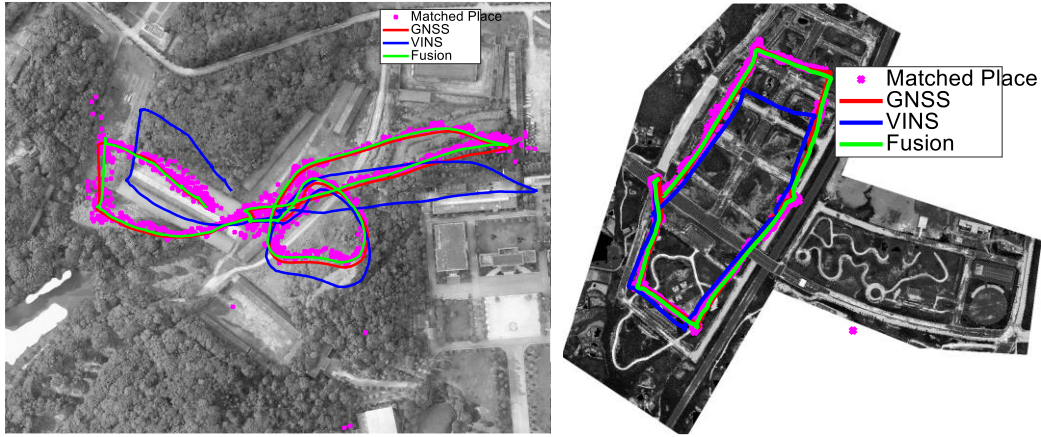


Figure 5. Demonstration of the localization results of the Rural (left) and the Testing Zone (right) datasets by plotting on the map. By fusing the relative localization results from the VIO and the absolute localization results from the aerial image registration, the proposed method achieves consecutive, drift-free and precise geolocalization performance.

proposed fusion method and the precision of its components in Table.III. As the initial position is unknown, the vehicle is not able to aware of its geodetic location before the first success georegistration; but once a georegistration is detected, the vehicle’s trajectory is transferred to align with the geodetic frame.

Note that, the VIO is not capable to measure the geodetic position. For fair comparisons, we moved its initial to aligned with the true geodetic initial position. It can be seen from Table.III that the VIO has the largest localization error in the two testing datasets, as its errors accumulate in the integration process. The absolute position obtained from areal image registration is much smaller than the VIO and it is drift-free. Fig.5 shows the registered places in the Rural and the Testing Zone datasets. The registered places distribute along the ground truth trajectory; however, the distribution is not smooth and there are also some wrong registrations distant to the ground truth trajectory. Such unsmooth and false localization results can bring in risks for the UAV control.

By fusing the relative and absolute localization results as described in section III.C, we achieve the best localization results. In the Rural dataset, the fused position error is 3.76 meters; while in the Testing dataset, the fused position error is 8.75 meters. The localization error from the pose graph optimization is much smaller than the VIO, as the pose graph incorporates aerial image registration to cure the drifts. Moreover, the fused results are also more accurate than the georegistration results; this is benefit from adding the relative constraints into the pose graph to achieve smooth localization performance. Note that, the wrong aerial image registration results have little influence on the optimized results, which demonstrates the advantage of using Huber loss in the objective functions as shown in (15).

In summary, by fusing the relative localization results from the VIO and the absolute localization results from the aerial image registration, we obtain consecutive, drift-free and precise geolocalization results. The proposed method can power various application of UAV and provides a novel solution to GNSS-denied autonomous navigation.

C. Comparing with Other Work

This part compares the experimental results with some other research published in recent years. Due to the lack of

publicly available code and dataset, we only summarize the reported localization performance and the corresponding experimental conditions. The details of the comparison are shown in Table IV.

It can be seen from Table IV that [9][11] and our method have integrated a dead reckoning component with the georegistration component to achieve consecutive and drift-free localization performance, while other work only focuses on georegistration. Note that, [9] used the Yamaha Rmax UAV, which is embedded with a relative good IMU, and [11] used tactical-level IMU for dead reckoning, while the proposed method combines a light-weighted MIMU with a camera to form a VIO. Note that, both our method and [11] incorporate 3D information in geolocalization. However, [11] requires a 3D map and known initial positions, while the proposed method only uses a 2D map with unknown initials. Though work with MIMU and 2D maps, the proposed method shows higher localization precision than the reported results in [9] and [11].

Our method’s localization accuracy in the Rural dataset is slightly lower than the results shown in [6] and [7]. However, we mounted the sensors rigidly to the UAV body, which is more challenging than using a gimbal based camera installation. Without unknown initials, the proposed method achieves comparable localization accuracy with [6] and [7], where a known initial position is required.

VI. CONCLUSIONS

In this paper, we have proposed a novel UAV localization method by using a camera, a MIMU, a magnetic compass, and a 2D georeferenced map. The method consists of three components: the visual-inertial odometry for relative localization, the aerial image registration for geolocalization and the pose graph for information fusion. The VIO provides relative motion constraints to the pose graph, while also reconstructs the 3D position of the observed features. Other than performing image-level registration, the proposed method aligns the reconstructed 3D points to the map points in the geodetic frame, which has shown a consistent high registration rate and a low geolocalization error. After obtaining the relative position from VIO and the geodetic position from the registration component, the pose graph component fuses them to achieve consecutive, drift-free and precise localization

performance. Comparing to existing work, the proposed method requires no prior knowledge of the initial position and achieves precise localization without using a gimbal; such a rigid sensor installation helps to fuse with sensors distributed at other parts of the vehicle. Future work can focus on using the odometry the bound the feature matching area, which can speed up the registration process and improve the registration success rate.

TABLE IV COMPARISON WITH STATE OF THE ART WORK

Author & Year	Localization Method	Experiments	Known initial	Accuracy
Conte et al. 2009 [9]	image registration + Kalman filter	Flight length: 1km; Flight height: 60 m; Sensors: good IMU and camera in a gimbal ; Map: 2D map;	Yes	<8m
Chiu et al. 2014 [11]	3D point registration + factor graph	Flight length: 26.5km; Flight height: --; Sensors: good IMU and camera; Map: 3D map	Yes	9.35m
Shan et al. 2015 [21]	image registration	Flight length: 0.72 km; Flight height: --; Sensor: camera; Map: 2D map	No	6.77m
Nasser et al. 2018 [12]	image registration	Flight length: --; Flight height: --; Sensor: camera; Map: 2D map	Yes	10.4m
Mantelli et al. 2019[10]	image registration	Flight length: 2.4km; Flight height: --; Sensor: camera in a gimbal ; Map: 2D map	Yes	17.78 m
Patel et al. 2020 [7]	image registration	Flight length: 1.1km; Flight height: 36-42m; Sensor: camera in a gimbal ; Map: 2D map	Yes	< 3m
Bianchi et al. 2021 [6]	Image registration	Flight length: 1.1km; Flight height: 36-42m; Sensor: camera in a gimbal ; Map: 2D map	Yes	< 3m
Ours	3D points alignment + pose graph	Flight length: 1.18/2.45km; Flight height: ~ 110/285m ; Sensor: MIMU and camera with rigid installation ; Map: 2D map	No	3.76/8.75m

ACKNOWLEDGEMENT

Thanks to Fan Chen, Wu Xuesong, Mao Dengke, Shang Hang and other colleagues' help in constructing the datasets.

REFERENCES

[1] C. Andy, A. Couturier, and M. A. Akhloufi, "A review on absolute visual localization for UAV," *Rob. Auton. Syst.*, vol. 135, p. 103666, 2021.

[2] D. Scaramuzza and F. Fraundorfer, "Visual odometry Part I: The First 30 Years and Fundamentals," *IEEE Robot. Autom. Mag.*, vol. 18, no. 4, pp. 80–92, 2011.

[3] D. Scaramuzza and Z. Zhang, "Visual-Inertial Odometry of Aerial Robots," *arxiv*, 2019.

[4] T. Qin, P. Li, and S. Shen, "VINS-Mono: A Robust and Versatile Monocular Visual-Inertial State Estimator," *IEEE Trans. Robot.*, vol. 34, no. 4, pp. 1004–1020, 2018.

[5] C. Campos, R. Elvira, J. J. G. Rodríguez, et al., "ORB-SLAM3: An Accurate Open-Source Library for Visual, Visual-Inertial and Multi-Map SLAM," *arxiv*, 2020.

[6] M. Bianchi and T. Barfoot, "UAV Localization Using Autoencoded Satellite Images," *IEEE Robot. Autom. Lett.*, pp. 1–8, 2021.

[7] B. Patel, T. D. Barfoot, and A. P. Schoellig, "Visual Localization with Google Earth Images for Robust Global Pose Estimation of UAVs," *IEEE Robot. Autom. Lett.*, pp. 6491–6497, 2020.

[8] G. J. J. van Dalen, D. P. Magree, and E. N. Johnsonz, "Absolute localization using image alignment and particle filtering," *2016 AIAA Guid. Navig. Control Conf.*, pp. 1–12, 2016.

[9] G. Conte and P. Doherty, "Vision-based unmanned aerial vehicle navigation using geo-referenced information," *EURASIP J. Adv. Signal Process.*, vol. 2009.

[10] M. Mantelli et al., "A novel measurement model based on abBRIEF for global localization of a UAV over satellite images," *Rob. Auton. Syst.*, vol. 112, pp. 304–319, 2019.

[11] H. Chiu, A. Das, P. Miller, et al., "Precise Vision-Aided Aerial Navigation," in *Proc. of the IEEE International Conference on Intelligent Robots and Systems (IROS)*, 2014.

[12] A. Nassar, K. Amer, R. Elhakim, and M. Elhelw, "A deep CNN-based framework for enhanced aerial imagery registration with applications to UAV geolocalization," *IEEE Comput. Soc. Conf. Comput. Vis. Pattern Recognit. Work.*, pp. 1594–1604, 2018.

[13] C. Cadena et al., "Past, present, and future of simultaneous localization and mapping: Toward the robust-perception age," *IEEE Trans. Robot.*, vol. 32, no. 6, pp. 1309–1332, 2016.

[14] C. Forster, Z. Zhang, M. Gassner, M. Werlberger, and D. Scaramuzza, "SVO: Semidirect Visual Odometry for Monocular and Multicamera Systems," *IEEE Trans. Robot.*, vol. 33, no. 2, pp. 249–265, 2017.

[15] J. Engel, V. Koltun, and D. Cremers, "Direct Sparse Odometry," *IEEE Trans. Pattern Anal. Mach. Intell.*, vol. 40, no. 3, pp. 611–625, 2018.

[16] R. Mur-Artal, J. M. M. Montiel, and J. D. Tardos, "ORB-SLAM: A Versatile and Accurate Monocular SLAM System," *IEEE Trans. Robot.*, vol. 31, no. 5, pp. 1147–1163, 2015.

[17] J. Surber, L. Teixeira, and M. Chli, "Robust visual-inertial localization with weak GPS priors for repetitive UAV flights," in *Proc. of the IEEE International Conference Robotics and Automation (ICRA)*, pp. 6300–6306, 2017.

[18] A. Yol, B. Delabarre, A. Dame, J. É. Dartois, and E. Marchand, "Vision-based absolute localization for unmanned aerial vehicles," in *Proc. of the IEEE International Conference on Intelligent Robots and Systems (IROS)*, pp. 3429–3434, 2014.

[19] G. Conte and P. Doherty, "An integrated UAV navigation system based on aerial image matching," in *Proc. of IEEE Aerospace Conference*, 2008.

[20] M. Calonder, V. Lepetit, C. Strecha, and P. Fua, "BRIEF: Binary robust independent elementary features," *Lect. Notes Comput. Sci.* vol. 6314 pp. 778–792, 2010.

[21] M. Shan, F. Wang, F. Lin, Z. Gao, Y. Z. Tang, and B. M. Chen, "Google map aided visual navigation for UAVs in GPS-denied environment," *arXiv*, 2015.

[22] D. G. Lowe, "Distinctive Image Features from Scale-Invariant Keypoints," *Int. J. Comput. Vis.*, vol. 60, no. 2, pp. 91–110, 2004.

[23] H. Kumar, "Geo-Registration of Aerial Images using RANSAC Algorithm," *NCTAESD*, pp. 234–238, 2014.

[24] Muja, Marius, and David G. Lowe. "Fast approximate nearest neighbors with automatic algorithm configuration," *VISAPP (2) pp.331-340*, 2009.